Modeling Spatio-temporal Assessment of Land Use Land Cover of Lahore and its impact on Land surface Temperature Using Multi-Spectral Remote Sensing Data

Aqil Tariq (aqiltariq@whu.edu.cn)

LIESMARS: Wuhan University State Key Laboratory of Information Engineering in Surveying Mapping and Remote Sensing
https://orcid.org/0000-0003-1196-1248

Faisal Mumtaz

Chinese Academy of Sciences

Research Article

Keywords: Land Surface Temperature (LST), Land Use Land Cover (LULC), CA-Markov Chain analysis, Maximum Likelihood Classification (MLC), Urban and Non-urban indices

Posted Date: May 24th, 2022

DOI: https://doi.org/10.21203/rs.3.rs-1587266/v1

Abstract

Urban sprawl, also widely known as urbanization, is one of the significant problems in the world. This research aims to assess and predict the urban growth and impact on Land Surface Temperature (LST) of Lahore as well as Land-Use and Land-cover (LULC) with a Cellular–Automata–Markov–Chain (CA–Markov–Chain). LULC and LST distributions were mapped using Landsat (5, 7, and 8) data from 1990, 2004, and 2018. Long–term changes to the landscape were simulated using a CA-Markov model at 14-year intervals from 2018 to 2046. Results indicate that the built-up area was increased from 342.54 (18.41%) km^2 to 720.31 (38.71%) km^2. Meanwhile, barren land, water and vegetation area was decreased from 728.63 (39.16%) km^2 to 544.83 (29.28%) km^2, from 64.85 (3.49%) km^2 to 34.78 (1.87%) km^2 and from 724.53 (38.94%) km^2 to 560.63 (30.13%) km^2 respectively. In addition, Urban Index, a non-vegetation index, accurately predicted LST, showing the maximum correlation R^2 = 0.87 with respect to retrieved LST. According to CA–Markov Chain analysis, we can predict the growth of built-up area from 830.22 km^2 to 955.53 km^2 between 2032 and 2046, based on the development from 1990 to 2018. As Urban Index as the predictor anticipated that the LST 20–23°C, and 24–27°C, regions would all decline in coverage from 5.30–4.79% and 15.79–13.77% in 2032 and 2046, while the temperature 36–39°C regions would all grow in coverage from 15.60–17.21% of the city. These findings are significant for the planning and development division to ensure the long-term usage of land resources for urbanization expansion projects in the future.

1. Introduction

According to the United Nations report of "World Organization Prospects 2014", almost half of the global population, approximately 3.7 billion, lives in cities (Kowalski, 2018). It is projected that the current population decline and unplanned population development will hit 66% (2.5 billion) by 2050 (Caselles et al., 1991; Lopez et al., 2001; Xue and Su, 2017). In recent decades, The rise in urban areas is about 90% of the population in Asia and Africa, in which Asia has a population of around 60% (4.5) billion (Reddy et al., 2014). This rapid population development is a historically anomalous problem because just 15% of the population living in Western Asian Regions by 1950 has risen to 35% by 2000 and is expected to a 54% increase by 2030 (Ahmed and Ahmed, 2012). It is also projected that from 2017 to 2050, it will add 750 million people and make Asia the second most significant contributor to the world's population. In developing countries, the urbanization rate is comparatively low. In 2000, 76% of people lived in urban areas, and by 2030, it is expected to rise to 83% (Walter, 2004; Wang et al., 2010). In 2000, just 40% of the population lived in cities and developed countries, increasing to 57% by 2030. Despite this rapid population increase in less established cities areas, it is estimated that the urbanization rate will double with a growth rate of 2.4% per annum between 2000 and 2030. However, the urbanization rate is expected to decline from 0.83–0.41% in developing countries between 2000 and 2030 (Gilani et al., 2020; Iram et al., 2012).

Despite their success in predicting trends of population development, only one analysis used indices of land cover to estimate projected distribution of Land Surface Temperature (LST) (Saitoh et al., 1996). While, the Normalized Difference Vegetation Index (NDVI) has been used to estimate residual city typical ecosystems and prospective LST values, the NDVI is thought to soak into large vegetation fractions, resulting in minimal temperature variation. In previous research, the Normalized Differentiate Built-up Index (NDBI) and Impervious Surface Areas (ISA) are better predictors of LST than the NDVI (Sobrino et al., 2013). The NDVI was calculated from a single satellite image (Ahmed et al., 2013), which is a method that is vulnerable to error because the season might vary greatly depending on the type of land cover. It is also necessary to alter the methodology by including seasonal estimates of land cover indices. Other analyses used linear regression to calculate LST on several indices, resulting in the NDVI, Soil Adjusted Vegetation Index (SAVI), Normalized Difference Built-up Area Index (NDBI), Urban Index (UI), Built-up-Index (BI), and Normalized Differentiate Water Index (NDWI) (Hasanlou and Mostofi, 2015). If several variables are included in a linear regression model, and the collinearity of the explanatory factors is high, the precision of the resulting dependent variable may be compromised (Ahmed et al., 2013). Environment predictions are as significant as they are dependable, but they suggest that a method for appropriately estimating LST without collinearity errors must first be identified.

Markov Chain Models (Ahmed and Ahmed, 2012; Araya and Cabral, 2010) have been used to predict LULC and urban expansion changes. Markov Chain analysis for Doha, Qatar, predicted a 21% increase in built-up area growth by 2020 (Hashem and Balakrishnan, 2015). Temperature predictions are made using both a global and a local model, which excludes metropolitan trends and considers their impact (Saitoh et al., 1996; Wilson, 2020). These models require further downscaling because they are at a coarse resolution (Hoffmann et al., 2012). Furthermore, global and regional models highlight temperature changes caused by greenhouse gas emissions, including temperature changes due to the impact of LULC changes. A Markov Chain-dependent model provides insights into possible thermal surface features due to changes in vegetation (Ahmed et al., 2013).

The research is suitable for predicting LST changes at the same spatio-temporal resolution with changes in LULC patterns, hence is able to model local and regional processes such as urban surface dynamics. Because of its prior successes in quantifying LULC alteration-related flexibility, effects, parsimony, and usefulness, the Markov Chain model has enormous predicting possible for future LST. By looking at past urban development patterns, this research can help us better understand how to predict future thermal city conditions. Many studies worldwide imply that development contributes to LST changes, but Pakistan currently lacks a body of knowledge on the subject. For the most part, the

country's meteorological research has relied on large-scale climate models and in-situ meteorological data, focusing primarily on precipitation and its agricultural implications (Charles et al., 2014; Manatsa et al., 2017; Mazvimavi, 2010). This area has had very few attempts to use remote sensing technology for climate research, especially at the microclimate levels found in metropolitan settings. Furthermore, urban development estimations based on remote sensing have focused on assessing the latest alterations in the LULC over the long term (Ahmed and Ahmed, 2012).

In Punjab, Pakistan, population development is rising and is weaker than in the other provinces. Lahore is the second-largest city in Pakistan after Karachi. Economic growth is increasing steadily due to certain factors such as industrialization and enhanced residential facilities that are a pull factor in the city's urban expansion (Nowak and Walton, 2005). Therefore, the rapid growth pace, its effect on vegetation, agricultural land, and quick change identification in Lahore city require testing. Local government and community planning can benefit this town's sustainable growth work. This work is essential to figure out the change in urban areas, the transformation of different land uses, and change detection of the urban sprawl in twenty-eight years. This study identifies the landcover-indices (NDVI, NDWI, SAVI, NDBI, and BI) using Landsat (TM, ETM+, and OLI) data representing correlations between LST and LULC changes in Lahore city from 1990–2018. Furthermore, the research found out which specific indices work well with the CA-Markov-Chain to predict the LULC and LST.

2. Material And Methods

2.1. Study area

Pakistan's second-largest city is Lahore which is located between 31°15' to 31°45'N and 74°01' to74°39' E. According to shapefile, the estimated area is 1860.55 km^2, with 217 meter elevations above sea level (Fig. 1) (Mumtaz et al., 2020). The District of Sheikhupura is in the north and west of the city of Lahore, bounded by Wagha at east and the district of Kasur in the south. Lahore became the capital of the province of West Punjab as the Indian subcontinent achieved independence in 1947. In 1955 it became the capital of the newly created province of West Pakistan which in 1970 was known as Punjab (Mosammam et al., 2017). Lahore has a tropical semi-arid climate with humid, long, and low summers, dry winter, monsoon, and dust storms. Lahore's environment becomes intense during the May, June, and July as temperatures increase to 36–42℃. The monsoon seasons commence from late June until August, with heavy rainfall throughout the northern and western provinces. The highest average temperature in town was reported on May 30, 2013, at 48.3 ℃ (118.9°F) and on June 10, 2016, 48 ℃ (118°F) (Tariq et al., 2020). The heat index in direct sunlight was recorded at 55°C (131°F) when the weather service in the shade officially recorded this temperature. The minimum temperature reported at Lahore city on January 13, 1967, is − 1.1 ℃ (30°F). The maximum reported 24-hour rainfall in the city is 221 mm (8.7 in), which occurred on August 13, 2008 (Tariq et al., 2020).

2.2. Data acquisition and Image Processing

Remote Sensing data combined with satellite imagery provides spectral, spatial, and temporal analysis for urban sprawl investigations and identifies LULC, LST, and spectral indices. Medium resolution multispectral satellite images were needed to measure the extent of the urban sprawl, LST, and LULC transition. Therefore, Landsat 5, 7, and 8 imagery were obtained from the online site of USGS-EROS (United States Geological Survey-Earth Explorer) website (https://www.usgs.gov/) with a cloud cover of less than 10% (Tariq and Shu, 2020). Table 1 displays the path, row, and acquisition dates of downloaded USGS datasets, accessible and readily available. We used the Fast Line-of-Sight Atmospheric Analysis of Spectral Hypercubes (FLAASH) module to make the atmosphere correction in ENVI v5.4 (Bernstein et al., 2005). Image analysis was performed after retrieving the images from the satellite, and image processing was conducted to use such images. Layer staking had been the first step in image processing. In ERDAS Imagine 2016, layer staking was performed to unite all the bands to shape a multispectral image. Landsat 7 data has missing data in straps form that should be removed before use. The 2004 satellite images SLC reflectors collected information from the surrounding pixels focal analysis from the spatial toolbox to fill the missing data (Weng et al., 2007). Land surface variations were predicted using satellite images from 1990, 2004, and 2018. These data were used to make the actual prediction. We used the same satellite images for the model efficiency according to Table 1. LULC and LST distributions were predicted using only one satellite image each year, which allowed the calculation of LST and non-urban indices.

Table 1
Landsat and ancillary data were used in this study.

Acquisition Date	Path	Row	Sensor	AT (°C)	RH (%)	Processing Level
1990-05-29	150	038	TM	34.4	54.0	TIER 1
2004-05-30	150	038	ETM+	36.3	56.0	TIER 1
2018-06-16	150	038	OLI/TIRS	38.7	57.0	TIER 1
(Note: AT: Air Temperature, RH: Relative Humidity).						

2.3. Land Use Land Cover (LU LC) mapping and accuracy assessment

Statistical grouping or grouping data image values (spectral pattern identification) into thematic groups or feature groupings are defined as classification. This technique aims to assemble and position all pixels with the same value in a single category/class. LULC maps for 1990, 2004, and 2018 were obtained from Landsat data using Maximum Likelihood Classification (MLC) algorithms. Four LULC categories: barren land, vegetation, built-up area, and water were acquired from each image as shown in Table 2 (Mushore et al., 2017).

Table 2
LULC types from the field survey in Lahore City.

LULC types	Details
Barren land	Areas with very low vegetation, shrubs, sparse grass and soil areas.
Vegetation	Areas covered with agriculture, grasslands, and thick trees characterized by high vegetation.
Built up area	Areas covered with residential, industrial and commercial activities.
Water/Wetland	Areas covered with wetland, lakes, ponds, river and all types of water bodies.

Assuming customarily distributed statistics for each class in each band, MLC estimates the likelihood that a given pixel belongs to one of many classes. ERDAS Imagine 2016 was used to classify the land use categories. In the training stage, analysis for each class was used to develop a statistical characterization signature editor (Hoffmann et al., 2012). These signatures are then used for supervised classification through signature allocation tools in the second stage. The final findings were then analyzed to examine twenty-eight years of improvements in LULC (Xu et al., 2013). We identified the changes of LULC and crossed match with Google Earth images. City shapefile were obtained from the Urban Unit for 1990, 2004, and 2018. They were checked by Google Earth, marked as built-up, and then exported to Arc Map 10.8 (Yuan and Bauer, 2007). Classified images for each year were assessed and displayed urban sprawl transition with its corresponding city boundary.

Thirty representative GPS locations per class were collected during an April-June 2018 field survey. We used training (70%) and testing (30%) samples for the accuracy assessment of LULC. Using shapefiles of each sample instead of points increases the accuracy of validation samples. LULC data from earlier research, aerial photographs, and topographical maps were used to generate ground-truth regions for assessing classification accuracy. Kappa coefficients (K) and Overall Accuracy (OA) were employed to evaluate the accuracy of LULC classifications. Every land cover class in Lahore was analyzed using post-classification (Jensen, 1983) variations between 1990 and 2018. Overall accuracy was determined by separating the cumulative number of pixels correctly identified from the cumulative number of pixels (Mumtaz et al., 2020) that could be written as N and Xii. Therefore, Xii = number of correctly labeled pixels, or the diagonal value, and N = cumulative number of pixels in the matrix. Kappa statistics incorporate the off-diagonal elements of the error matrices (Mushore et al., 2017). It was calculated by using the following Eq. 1:

$$K = \frac{N\sum_{i=1}^{i} Xii - \sum_{i=1}^{r}(x_{i+} \times x_{+i})}{N^2 - \sum_{i=1}^{r}(x_{i+} * x_{+i})} (1)$$

Where r is the number of rows in confusion matrix Xii the number of observations in row i and column i (along the major diagonal); x_{i+} is the marginal total of row i; x_{+i} are the marginal totals of column i and N is the total number of observations.

2.4. Estimation of LST using Landsat data

Thermal bands from Landsat 5 and 7 (B# 6) and Landsat 8 (B# 10) were used to determine LST for each year. Images taken in May and June were utilized to minimize the impact of seasonality. Landsat 8 has two thermal bands (B10 and B11). In this study, We used band 10 to estimate LST (Datta et al., 2017). To acquire LST from brightness temperature maps, digital values have to be converted to radiances. Radiance and emissivity data were used to adjust brightness temperature calculations (Jimenez-Munoz et al., 2014; Sobrino et al., 2004; Tariq et al., 2020). When converting digital numbers (DN) to radiance (L_λ), an ArcMap 10.8 addition called the Reflectance toolbox was utilized. The utility used metadata files to extract parameters and apply them to thermal data. Eq. (2), a single-channel Landsat estimate of Planck's blackbody temperature, was used to obtain T_B from thermal radiance (Deilami et al., 2018; Stathopoulou et al., 2006).

The Landsat Surface Temperature (LST) was calculated using geometrically corrected Landsat satellite images taken in 1990, 2004, and 2018. The LST was calculated using Eq. 2 (Weng et al., 2004). For each pixel, digital number (DN) was converted into the radiance (L_λ) as follows:

$$L_\lambda = \left(\frac{L_{max\lambda} - L_{min\lambda}}{Q_{Calmax} - Q_{Calmin}} \right) \times (Q_{Cal} - Q_{Calmin}) + L_{min\lambda} (2)$$

where $L_{max\lambda}$ and $L_{min\lambda}$ are the maximum and minimum radiance values, $QCAL_{max}$ the maximum quantized calibrated pixel value (corresponding to $L_{max\lambda}$ in DN (255)), $QCAL_{min}$ is the minimum quantized calibrated pixel value (corresponding to $L_{min\lambda}$ in DN (01)) respectively; and their values were available from the metadata of the Landsat images. Secondly, the L_λ values were converted into brightness temperature (T_B) as follows:

$$T_B = \left(\frac{K_2}{ln\left(\frac{K_1}{L_\lambda} + 1\right)} \right) - 273.5 (3)$$

Where K_1 and K_2 are constant and available from the United States Geological (See Table 3). From every thermal band, we identified from spectral radiance and black body the pixel-based land surface emissivity map (ε), as developed (Yang, 2004) and also applied recently (Mushore et al., 2018). Ultimately, real LST was obtained using Eq. (3) after emissivity correction (ε) was applied to the brightness temperature (Weng et al., 2007).

Table 3
Thermal band rescaling and calibration constants of Landsat data were used in this study

Sensor	K_1 Watts (meter^2 *ster *μm)	K_2 (meter^2 *ster *μm)	Rescaling
TM	607.76	1260.56	
ETM+	666.09	1282.71	
OLI/TIRS	774.8853	1321.0789	M_L 0.0003342 A_L 0.10

$$LST = \frac{T_B}{\left[1 + \left[\frac{\lambda T_B}{p}\right] ln\epsilon\right]} (4)$$

The sign λ denotes the wavelength of the emitted thermal radiance (11.5μm), and the symbol p denotes the wavelength of the emitted thermal radiance 1.438×10^{-2mk}. We collected LST data for all dates corresponding to the images shown in Table 3 below.

To predict LST, training models use long-term temperature fluctuations as a visual cue. Thermal data for 1990, 2004, and 2018 were used to calculate the LST (Table 1). To see if urbanization was still raising the LST, and if so, what kind of development might be on the horizon, this study was carried out in the first place.

2.5. Calculation of urban and non-urban indices

Temperature fluctuations across the season were explained using the LST. The average LST for 1990, 2004, and 2018 was calculated using Table 1. This experiment was conducted to see if LST changed due to urban expansion (Xu et al., 2013). The approach (Smakhtin and Hughes, 2007) estimated barren land, vegetation, built-up area, and water bodies. Fu's approach created the land cover index maps (Fu and Weng, 2016). LST was computed using Landsat satellite images taken in 1990, 2004, and 2018 that had been geometrically adjusted (Hasanlou and Mostofi, 2015). The indices of urban an dnon-urban indices formulas in Table 4were used to corelatewith the LST.

Table 4
Calculation of urban and non-urban indices was used in this study area.

Abbreviations	Indices	Formulation (Landsat 5 and 7)	Formulation (Landsat 8)	References
NDVI	Normalized Difference Vegetation Index	$\frac{(Band4-Band3)}{(Band4+Band3)}$ $\frac{(\mathrm{NIR}-\mathrm{Red})}{(\mathrm{NIR}+\mathrm{Red})}$	$\frac{(Band5-Band4)}{(Band5+Band4)}$ $\frac{(NIR-Red)}{(NIR+Red)}$	(Tucker, 1979)
NDWI	Normalized Difference Water Index	$\frac{(Band3-Band5)}{(Band3+Band5)}$ $\frac{(\mathrm{Red}-\mathrm{SWIR1})}{(\mathrm{Red}+\mathrm{SWIR1})}$	$\frac{(Band4-Band6)}{(Band4+Band6)}$ $\frac{(Red-SWIR1)}{(Red+SWIR1)}$	(McFeeters, 1996)
SAVI	Soil Adjusted Vegetation Index	$\frac{(\mathrm{Band4}-\mathrm{Band3})}{(\mathrm{Band4}+\mathrm{Band3}+\mathrm{L})}\times(\mathrm{L}+1)$ $\frac{(NIR-RED)}{NIR+RED+L}\times(L+1)$	$\frac{(\mathrm{Band5}-\mathrm{Band4})}{(\mathrm{Band5}+\mathrm{Band4}+\mathrm{L})}\times(\mathrm{L}+1)$ $\frac{(NIR-RED)}{NIR+RED+L}\times(L+1)$	(Huete, 1988)
NDBI	Normalized Difference Built-up Area Index	$\frac{(Band5-Band4)}{(Band5+Band4)}$ $\frac{(SWIR1-NIR)}{(SWIR1+NIR)}$	$\frac{(Band6-Band5)}{(Band6+Band5)}$ $\frac{(SWIR1-NIR)}{(SWIR1+NIR)}$	(Zha et al., 2003)
BI	Bare Soil Index	$\frac{(Band5+Band3)-(Band4+Band1)}{(Band5+Band3)+(Band4+Band1)}$ $\frac{(SWIR1+RED)-(NIR+Blue)}{(SWIR1+RED)+(NIR+Blue)}$	\frac{\left(Band6+Band4\right)-\left(Band5+Band2\right)}{\left(Band6+Band4\right)+\left(Band5+Band2\right)} \frac{\left(SWIR1+RED\right)-\left(NIR+Blue\right)}{\left(SWIR1+RED\right)+\left(NIR+Blue\right)}	(Mann and Whitney, 1947)

2.6. Temperature prediction using various parameters

The LST computation requires a strong correlation between the LST and the predictor selected variables, with no collinearity among them. It was determined by using the indices listed in Table 4. A linear regression model was used to predict LST using spectral indicators with the highest correlation. The correlation between such variables was also examined to avoid tightly clustered predictors, which could cause collinearity-related mistakes. To create a multivariate linear model, we picked indicators that were substantially connected with LST and poorly correlated with each other. We used the model to test its performance to predict 2018 observed LST. Accuracy was measured using Mean-Absolute-Percentage-Error (MAPE) shown in Eq. (5) (Mann and Whitney, 1947).

$$\mathrm{MAPE}\left(\%\right)=\frac{1}{N}\sum_{i=1}^{N}\left(\left|\frac{T_{predicted}-T_{observed}}{T_{observed}}\right|\right)_{i}\times 100 \quad (5)$$

where $T_{observed}$ is the real ith pixel of LST reported and $T_{predicted}$ is the model surface temperature from Landsat info. Error is expressed in percentages using the absolute mean percentage of the accuracy statistic. It was determined that the model's accuracy in predicting temperature could be quantified by calculating the Root Mean Square Error (RMS), Nash-Sutcliff performance, Agreement-Index (A-I), and Mean Bias Error (MBE). LST distribution for 2032–2046 was predicted using a model evaluated for accuracy. The 14 years were chosen since the analysis demonstrated significant changes at the same points in time.

2.7. LULC changes and modeling for 2032 and 2046

The LULC has been represented using various predictive models (Triantakonstantis and Mountrakis, 2012). CA-Markov chain analysis can forecast the possible distribution of LULC and LST based on remote sensing data (Mumtaz et al., 2020; Tariq and Shu, 2020) indicated in Fig. 2. It was compared to a genuine 2004 map for comparison. A 2018 state simulation was run during this study to verify that the expected LST distribution was in line with the actual distribution. Detailed explanations of the proposed actions can be found in sections 2.7.1 and 2.7.2.

2.7.1. CA-Markov chain analysis to predict LULC changes

The Markov model permits the structure to advance from the initial state *i* to *j* during a time period *T* (Hashem and Balakrishnan, 2015). Markov Chain was chosen for its ability to anticipate time changes in LULC (Araya and Cabral, 2010; Triantakonstantis and Mountrakis, 2012). In addition, the Markov Chain can predict complicated system fluctuations (Tariq and Shu, 2020; Triantakonstantis and Mountrakis, 2012). CA-Markov chain models were used in IDRISI software Selva v 17.0 to forecast the distribution of LULC in 2018, 2032, and 2046 (Arsanjani et al.,

2012; Hou et al., 2019; Mosammam et al., 2017; Sayemuzzaman and Jha, 2014). Future land cover distributions can be predicted using a Cellular Automata (CA) model that incorporates probability derived from the Markov Chain analysis. As a result, the combination of Markov Chain and Cellular Automata revealed changes in land change cover over time. A CA-Markov Chain was used to test their capacity to anticipate future LULC trends in dynamic metropolitan environments. The 2018 LULC distribution was predicted using LULC shifts from 1990 to 2004, and the distribution was compared to LULC transformations from 1990 to 2004. The MLC classifications were used to compare the expected land use and land cover with the actual shape in 2018. For 2018, the Kappa-Agreement-Index (KIA) measured the degree of agreement between maps of the same instance from 1990 to 2004 (Arsanjani et al., 2012). The KIA was used to evaluate the CA-predicting Markov's ability by comparing the 2018 MLC classification map to the 2018 predicted map. After assessing the accuracy of the CA-Markov-Chain model, we employed LULC patterns from 2004 and 2018 to predict the terrain for the years 2032 and 2046, to no avail.

2.7.2. CA-Markov of indices for the prediction of LST

Section 2.7 defines the Urban Indices (UI) as the most robust predictor variable of LST distribution. Table 8 in section 3.3 shows the success of various land-cover indices in predicting LST and how that contributes to UI selection through land-cover indices. Satellite images were taken in May and June in 1990, 2004, and 2018, resulting in an average user interface (UI) each year (Table 1). Data from 1990 and 2004 average UIs were used to generate change probability matrices for the CA model, which predicted the possible condition of the index for 2018. Results from CA-Markov chains also employed 1990 and 2018 means of urban indices to estimate the UI status in 2032 and 2046. Predictions of LST for 2018, 2032, and 2046 were made using a linear regression model (section 3.4). Urban Indices maps were reclassified into a model to predict the temperature classes of 20–23°C, 24–27°C, 28–31°C, 32–35°C, and 36–39°C as predicted by CA-Markov Analysis. LST predictions for Lahore city for 2032 and 2046 were the results of this phase.

2.7.3. Statistical importance of examining LULC and LST

Predicted changes in LULC and LST distribution were examined for their statistical significance. Coded LULC readings and temperature levels produced from 300 locations were tested. Each period, the LST groups were classified 1–5, whereas the LULC levels were coded 1–4 according to Markov analysis criteria and performance. The Shapiro-Wilk statistic was employed to assess for regularity in the earliest stages of the study (Shapiro And Wilk, 1965). A Mann Whitney test was used to determine the significance of LULC and LST deviations (Birnbaum, 1956; Mann and Whitney, 1947). We verified that the Ha hypothesis concerning LULC and LST spatial distributions is distinct from the alternative Hb theory: in 2018 and 2046, the pairs of LULC and LST were not identical (Mushore et al., 2017).

3. Results And Discussion

3.1. Spatio-temporal LULC changes with accuracy assessment

Results in Fig. 3 indicates the LULC variations of the Lahore region for the years 1990, 2004, and 2018. Figure 3a clearly explains significant changes in the built-up area in the middle of the city in 1990, while growth in a built-up area and low vegetation index for 2004 (Mallick et al., 2008). Figure 3b indicates that the built-up area was concentrated in the district's center. However, tiny pockets of built-up areas could still be found simultaneously in substantial numbers across the map. Similarly, a lower vegetation index, high built-up area were observed for 2004. It was likely due to reduced rainfall. Figure 3c demonstrates the 2018 area of land use separation. During 2018, the built-up area amplified considerably due to establishing housing schemes in Lahore and other cities from 2004 to 2018 (Butt et al., 2015). Our results indicate that vegetation cover decreased in Lahore and other neighboring cities.

As seen in Table 5, there have been significant changes in LULC distribution between 1990 and 2018 using the MLC algorithm. Most of the changes in agriculture/vegetation and the urban environment. It should be noted that from 1998 to 2004, the rise in the built-up area was very high, but after that, the development in the built-up area was slow until 2018. The above data were validated by previous knowledge and Google Earth images (Mumtaz et al., 2020; Tariq et al., 2020). The built-up area was increased from 342.54 (18.41%) to 720.31 (38.71%) km^2. Meanwhile, barren land, water and vegetation area was decreased from 728.63 (39.16%) to 544.83 (29.28%) km^2, from 64.85 (3.49%) to 34.78 (1.87%) km^2 and from 724.53 (38.94%) to 560.63 (30.13%) km^2 respectively (Table 5).

Table 5
Spatio-temporal changes of LULC from 1990–2018.

LULC	Land use classification in Lahore (Area in Km^2 (%))			Change detection (Area in Km^2 (%))		
	1990	2004	2018	1990–2004	2004–2018	1990–2018
Barren Land	728.63 (39.16)	653.12 (35.10)	544.83 (29.28)	-75.51 (-4.06)	-108.29 (-5.82)	-183.80 (-9.88)
Vegetation	724.53 (38.94)	650.25 (34.95)	560.63 (30.13)	-74.28 (-3.99)	-89.62 (-4.82)	-163.90 (-8.81)
Built up area	342.54 (18.41)	501.25 (26.94)	720.31 (38.71)	158.71 (8.53)	219.06 (11.77)	377.77 (20.30)
Water	64.85 (3.49)	55.93 (3.01)	34.78 (1.87)	-8.92 (-0.48)	-21.15 (-1.14)	-30.07 (-1.62)
Total Area	1860.55 (100)	1860.55 (100)	1860.55 (100)	0.00 (0.00)	0.00 (0.00)	0.00 (0.00)

Different measures were used to assess the accuracy of the MLC classification to categorize into the four LULC types. The highest overall accuracy (OA) value, i.e., 98%, was obtained from the 1990 LULC image, while the 2004 image had the lowest OA of 93%. The highest UA of the vegetation area class was attained for the 2008 image, with 99.06%, while the lowest was 75.03% for the 'water' class for the image taken during 2004. The OA and K for Lahore District as a whole are 0.98 and 0.97 (corrected samples, 201), 0.97 and 0.95 (fixed samples, 181), 0.93 and 0.89 (selected samples, 178) for 1990, 2004, and 2018, respectively (Table 6).

Table 6
Accuracy assessment of LULC from 1990–2018.

Classes	1990				2004				2018			
	UA	**PA**	**OA**	**K**	**UA**	**PA**	**OA**	**K**	**UA**	**PA**	**OA**	**K**
Barren land	98.77	97.56	0.98	0.97	66.67	92.53	0.97	0.95	96.77	94.26	0.93	0.89
Vegetation	99.03	98. 08			98.37	96.80			99.06	97.22		
Built up	98.08	95.30			96.30	95.65			95.12	97.50		
Water	90.00	94.74			75.03	79.03			87.29	89.01		
PA: Producer Accuracy, UA: users Accuracy, OA: Overall Accuracy, Kc: Kappa Coefficient												

3.2. Observed LST changes from 1990-to 2018 using Landsat data

There has been a significant rise in Lahore's long-term LST since 1990. Figure 4 shows that in 1990, in contrast to succeeding years, the region was primarily covered by temperatures between 20–23°C and 24–27°C. Although lower surface temperatures were found in several areas of the main research area in 2018, the 36–39°C group was most prevalent in 2018. Temperature rises were more significant in the built-up areas of the center than in the surrounding areas of vegetation, water, and barren land. Figure 4a is satellite-derived land surface temperature. Figure 4a shows that in 1990 built-up areas were not too much, so the temperature was also low towards the boundary. In most areas, the temperature was between 20–23°C and 24–27°C.

Figure 4b shows that in 2004, the built-up area had increased so as the temperature was also high towards the boundary. Figure 4c shows that in 2018, the built-up area had increased, so the temperature was also high towards the boundary. The temperature was between 32–35°C to 36–39°C in almost 1/3 area of the city. The low-temperature area had decreased over time, and the high-temperature area had been reduced due to an increase in the urban area in the middle of the city. In 2018, temperature was 36–39°C in Lahore city. In 1990, most of the area had a temperature of between 20–23°C. The temperature is 32–35°C; the temperature has risen 12°C because of urban areas for twenty-eight years.

Table 7 summarizes the variations in LST between 1990 and 2018. The percentage of LST in the 20–23°C temperature range declined by roughly 37% as the city grew. A significant changes and rise in the (35–42°C) high LST coverage over this time period suggests that Lahore city is experiencing substantial warming of the earth.

Table 7
Average LST responses to urban expansion in Lahore city.

LST °C	LST area in km^2 (%)		
	1990	2004	2018
20–23	103.77 (5.58)	343.17 (18.44)	114.16 (6.14)
24–27	1026.36 (55.16)	399.41 (21.47)	325.68 (17.50)
28–31	614.91 (33.05)	344.38 (18.51)	405.51 (21.80)
32–35	110.75 (5.95)	639.27 (34.36)	761.85 (40.95)
36–39	4.77 (0.26)	134.33 (7.22)	253.35 (13.62)

3.3. Measurement of Coefficient of determination for LST with Normalized Satellite Indices

Table 8 shows the yearly variability in LST regarding multiple normalized satellite indices of the Lahore region for 1990, 2000, and 2018. The results show that the annual variability in LST has increased in the last three decades. The LST exhibits substantial interannual variability concerning yearly scales compared to the NDVI, NDWI, SAVI, NDBI, and BI variables. The yearly scale (between 1990 and 2004) revealed a statistically significant positive link between LST and SAVI, NDBI and BI for the regions located in the central portion of Lahore city, while NDVI and NDWI have a negative association with LST. Negative trends have been seen in the western and the upper part of the Lahore city. A lack of vegetation in these places has contributed to significant changes in temperature. In contrast, an inverse link was detected in a small region (NDVI) of the eastern continent, where it is challenging to evaluate LST patterns due to the lack of vegetation. There is a strong correlation between LST and the many factors assessed every year. In 2018, LST and indices have shown a 77.2% increase in favorable trends (Das et al., 2021).

Table 8
Coefficient of determination for LST Normalized Satellite Indices.

Years	Indices	LST	NDVI	NDWI	SAVI	NDBI	BI
1990	LST	1.0000	−0.7133	0.6120	0.7191	0.8801	0.7461
	NDV I	−0.7133	1.0000	−0.7956	0.9138	−0.8556	−0.8148
	NDWI	0.6120	−0.7956	1.0000	−0.8674	0.6455	0.5870
	SAVI	−0.7191	0.9138	−0.8674	1.0000	−0.9398	−0.9018
	NDBI	0.8801	−0.8556	0.6455	−0.9398	1.0000	0.9828
	BI	0.7461	−0.8148	0.5870	−0.9018	0.9828	1.0000
2004	LST	1.0000	−0.5353	−0.1700	0.6353	0.9907	0.7461
	NDV I	−0.5353	1.0000	−0.7157	1.0000	−0.7698	−0.8148
	NDWI	−0.1700	−0.7157	1.0000	−0.7157	0.1052	0.8151
	SAVI	−0.6353	1.0000	−0.7157	1.0000	−0.7698	0.4390
	NDBI	0.9907	−0.7698	0.1052	−0.7698	1.0000	0.5870
	BI	0.8462	0.3237	−0.7899	0.3237	0.2603	1.0000
2018	LST	1.0000	-0.0455	-0.7230	0.8962	0.6276	0.8918
	NDVI	−0.7157	1.0000	−0.9040	−0.8918	−0.1424	−0.8148
	NDWI	0.3073	0.4390	1.0000	0.9541	0.1084	−0.0322
	SAVI	0.1052	−0.0322	−0.1059	1.0000	0.1202	−0.7956
	NDBI	0.8275	−0.3435	0.9098	0.7413	1.0000	−0.9040
	BI	0.4324	−0.1059	0.8151	0.9316	0.3390	1.0000

3.4. Calculation of LST from UI

Figure 5 depicts the linear regression model for predicting the LST based on the Urban Indices (UI). Since surface temperature and UI had R^2 value of 0.87, the correlation was too significant. Thus, LST and UI had improved and did not affect their association due to saturation that disturb indices like NDVI, as the UI continuous to increase with abundant temperature.

In 2018, the linear regression model was tested using Landsat data. This was very much in line with the known trends of temperature (Fig. 6). Tsat is the satellite-observed temperature, while Tmod is the derived temperature from the model. The UI temperature and Landsat 8 thermal data were analyzed to compare the two results based on 300 sites in the area of research studied (Fig. 1).

3.5. LST and LULC prediction for 2032 and 2046

3.5.1. Accuracy Assessment of Cellular Automata Markov Chain LULC for 2032 and 2046

Analyzing the data visually revealed a correlation between the MLC classifier's estimate for 2018's LULC distribution and the CA-Markov model's prediction for 2018 (Fig. 7). A set of in-situ measurements drives the model to reproduce the MLC-defined spatio-temporal dispersion of LULC. CA-KIA Markov's prediction for LULC was 0.88, while MLC's classifier predicted a dispersal of 0.85 using KIAs (Table 9). Vegetation and water classes on both maps agreed most strongly (KIA = 0.81), with the weakest (KIA = 0.79).

Table 9
Correlation analysis between MLC and CA-Markov Chain based on 2018 prediction.

LULC	Kappa Index of Agreement (KIA)
Barren land	0.85
Vegetation	0.81
Built-up area	0.86
Water/Wetland	0.79

3.5.2. Prediction and distribution of LULC and LST in Lahore before 2046

Figure 8 displays in 2032 and 2046, the CA-Markov-Chain model predicted an increase in built-up areas associated with barren land, vegetation, and water. Buildings may eventually overtake parks if current trends continue, as they have in the past. Table 10 shows that the extent of built-up area is probably to increase from where they are now until 2046. According to the CA-Markov model, built-up areas are likely to grow from 830.22 km^2 to 955.53 km^2, while vegetation area decreased from 478.91 km^2 to 402.83 $km^2$from 2032 to 2046. Based on model predictions, expansion in built-up areas and decreases in water, vegetation, and barren land regions are the primary drivers of future development.

Table 10
Prediction of LULC types and LST between 2032 and 2046.

LULC	LULC area in km^2 (%)		LST (°C)	LST area in km^2 (%)	
	2032	2046		2032	2046
Barren Land	478.91(25.75)	402.83 (21.66)	20–23	98.68 (5.30)	89.08 (4.79)
Vegetation	530.27(28.51)	487.42 (26.20)	24–27	293.80 (15.79)	256.22 (13.77)
Built up area	830.22 (44.63)	955.53 (51.37)	28–31	333.73 (17.94)	314.99 (16.93)
Water	20.68 (1.11)	14.30 (0.77)	32–35	844.10 (45.37)	880.09 (47.30)
Total Area	1860.08 (100)	1860.08 (100)	36–39	290.25 (15.60)	320.17 (17.21)

Figure 8 illustrates the LST growing trend from 2032–2046. The model explained LST variations between 2032 and 2046 due to increased built-up area. The size of high LST (more than 36°C) in (Figs. 8a–b) was projected to increase at the cost of lower LST classes. Thus, western and northern areas with vegetation were cooler than built-up areas. Maximum area with low LST (20–23°C and 24–27°C) were moved to the high LST class area (32–35°C and 36–39°C). Most of the areas, particularly in the northwestern and central areas, could shift towards high temperature (more than 36°C), whereas the size of low LST classes (20–23°C and 32–35°C) may decrease (Table 10).

From 2032 to 2046, the model indicated that the temperature ranges from 24–27°C would decline by 293.80–256.22km^2, while the LST ranges from 36–39°C are expected to rise by 290.25–320.17km^2. In the long run, temperatures in the high category (over 26°C) are anticipated to grow at the expense of those in the lower category, as shown in Figs. 8 (a–b). There will be a significant increase in temperature in the built-up area. It is expected that most of the low LST (20–23°C and 24–27°C) would turn high LST (32–35°C and 36–39°C) locations. While the amount of lower LST (20–23°C or 24–27°C) may diminish, many places, notably in the center and northwestern area, could shift toward warmer temperatures (more than 36°C), as shown in Table 10.

The urban land use information is critical to city population activity monitoring, government policy-making, and urban management. However, the density of urban systems makes it challenging to classify urban functional zones accurately. Most urban land use classification studies have used features extracted from social media data and high, medium, and low spatial resolution satellite images (Peña, 2008). Still, only a few have used both features simultaneously because there are not any models available for them to use (Pal and Ziaul, 2017).

Land System Science (LSS) is at the forefront of research to generate much-needed knowledge that can help find land-related pathways to sustainable development (Li et al., 2016). According to Land System Science, human use of land is a social-ecological system with several interconnected components that influence each other (Baqa et al., 2021; Shi et al., 2019; Tariq et al., 2021). Land system scientists examine the implications for sustainable development through the lens of inter and intragenerational justice, emphasizing the importance of incorporating multiple actor perspectives (especially those of local communities) (Hamza et al., 2021). People need to have a good quality of life now and in the future, but they also need to keep the environment safe.

To achieve many of these objectives, competing claims on land are at the heart of many related disputes (Elliott and Frickel, 2015; Hasanlou and Mostofi, 2015). A variety of interests, ranging from residents to multinational corporations, vie for control of and access to land, including the security of their livelihoods, sense of place, economic assets, preservation of natural habitats, and their claim to territorial sovereignty. These competing interests range from the local to the international (Ahmed et al., 2013; Sayemuzzaman and Jha, 2014; Sultana et al., 2014). It is possible to see the recent changes in Pakistan's land use and governance patterns as a manifestation of these actors' power dynamics. People cut down trees, made big plantations for commercial monocultures, and set up special economic zones. More non-governmental organizations (NGOs) concerned with forest conservation are some of the effects of these land-use changes in Pakistan, one of the world's biodiversity hotspots (Ma and Tong, 2022; Prasad et al., 2022; Zahoor et al., 2022). This article's overall goal is to investigate the links between sustainable development outcomes and recent land-use changes to identify leverage points and priority areas of concern for more sustainable land governance in Lahore city, Pakistan. If Pakistan doesn't properly manage the many conflicting claims on land, it won't be able to meet its 2030 Agenda goals.

4. Conclusions

This research was carried out to evaluate urban growth phenomena and their impacts on vegetation land and change in temperature from 1990 to 2018. RS and GIS techniques were used to analyze the spatiotemporal patterns of land use. LST and LULC distributions in Lahore will be predicted using a new CA-Markov-Chain developed in this research. For urban areas categorized using Landsat 5, 7, and 8 imagery, we observed that the MLC method utilized obtained an overall accuracy of above 80% when applied. According to MLC classifications of LULC types, in situ measurements could drive the model's ability to reproduce the LULC types' spatio-temporal distribution accurately. It was shown that the CA-Markov model predicted a KIA of 0.88 and 0.85 between the LULC and the distribution obtained using the MLC classifier. This analysis can predict the growth of built-up area from 830.22 km^2 to 955.53km^2 between 2032 and 2046, based on the development from 1990 to 2018. Considering the CA-Markov Chain models based on UI anticipated that the temperature 20–23°C and 24–27°C regions would all decline in coverage from 5.30–4.79% and 15.79–13.77% in 2032 and 2046, while the temperature 36–39°C regions would all grow in coverage from 15.60–17.21% of the city.

As a result of increased urbanization in Lahore, the observed values between 1990 and 2018 in the categories 20–23°C and 24–27°C declined by roughly 37% and 22%, respectively, indicating a severely biased trend of land heating in Lahore city. Only the effects of urban development on temperature variations are considered in the model, which is limiting. However, there has been a minor shift in LST patterns due to successful mitigation policies and innovative urban expansion methods. In general, the outcomes of this study show the utility of medium-resolution satellite data in estimating possible land surface temperatures in urbanized areas. In the absence of control measures, we conclude that urbanization will enhance warming and increase temperatures in the future. Urban planners must be warned of urban dwellers' potential

temperature fluctuations and thermal comfort due to growth based on this study. Meanwhile, more research is needed to see if these methods and procedures can be applied globally and nationally. The CA model and Markov Chain analysis were employed to identify spatial distribution changes and forecast time resolution. This model will be used in the future by researchers and policymakers to develop new policies to control and manage urban expansion.

Declarations

Availability of data and material

The datasets generated and/or analyzed during the current study are not publicly available but are available from the corresponding/first author on reasonable request.

Ethics declarations

Ethics approval and consent to participate

The facts and views in the manuscript are solely ours, and we are responsible for authenticity, validity, and originality. We also declare that this manuscript is our original work, and we have not copied it from anywhere else. No plagiarism is detected in this manuscript.

Consent for publication

We undertake and agree that the manuscript submitted to your journal has not been published elsewhere and has not been simultaneously submitted to other journals.

Competing Interests

The authors declare no conflict of interest.

Funding

This work is supported by the National Natural Science Foundation of China (grant no. 41901292 and 42071321).

Author Contributions

Aqil Tariq conducted the overall analysis and led the writing of the manuscript, design and data analysis. Aqil Tariq and Faisal Mumtaz provided technical inputs for the research, and reviewed the paper. All authors have read and agreed to the published version of the manuscript.

Acknowledgments

We would like to pay special and heart whelming thanks to NASA-Earth data for providing us Landsat data and Clark Labs for providing us IDRISI Selva v_17.0 for analysis. The authors would like to thank Stephen C. McClure for his enthusiastic support and valuable suggestions during the review and also improved the language of the manuscript. We also thankful for both reviewers and editor for valuable suggestions and comments.

References

1. Ahmed B, Ahmed R (2012) Modeling urban land cover growth dynamics using multioral satellite images: A case study of Dhaka, Bangladesh. ISPRS Int J Geo-Information 1:3–31. https://doi.org/10.3390/ijgi1010003
2. Ahmed B, Kamruzzaman MD, Zhu X, Shahinoor Rahman MD, Choi K (2013) Simulating land cover changes and their impacts on land surface temperature in dhaka, bangladesh. Remote Sens 5:5969–5998. https://doi.org/10.3390/rs5115969
3. Araya YH, Cabral P (2010) Analysis and modeling of urban land cover change in Setúbal and Sesimbra, Portugal. Remote Sens 2:1549–1563. https://doi.org/10.3390/rs2061549
4. Arsanjani JJ, Helbich M, Kainz W, Boloorani AD (2012) Integration of logistic regression, Markov chain and cellular automata models to simulate urban expansion. Int J Appl Earth Obs Geoinf 21:265–275. https://doi.org/10.1016/j.jag.2011.12.014
5. Baqa MF, Chen F, Lu L, Qureshi S, Tariq A, Wang S, Jing L, Hamza S, Li Q (2021) Monitoring and modeling the patterns and trends of urban growth using urban sprawl matrix and CA-Markov model: A case study of Karachi, Pakistan. https://doi.org/10.3390/land10070700. Land 10
6. Bernstein LS, Adler-Golden SM, Sundberg RL, Levine RY, Perkins TC, Berk A, Ratkowski AJ, Felde G, Hoke ML (2005) Validation of the QUick atmospheric correction (QUAC) algorithm for VNIR-SWIR multi- and hyperspectral imagery. Algorithms Technol. Multispectral,

Hyperspectral, Ultraspectral Imag. XI 5806, 668. https://doi.org/10.1117/12.603359

7. Birnbaum ZW (1956) On a use of the Mann-Whitney statistic, in: Proceedings of the Third Berkeley Symposium on Mathematical Statistics and Probability, Volume 1: Contributions to the Theory of Statistics. The Regents of the University of California
8. Butt A, Shabbir R, Ahmad SS, Aziz N (2015) Land use change mapping and analysis using Remote Sensing and GIS: A case study of Simly watershed, Islamabad. Pakistan Egypt J Remote Sens Sp Sci 18:251–259. https://doi.org/10.1016/j.ejrs.2015.07.003
9. Caselles V, López García MJ, Meliá J, Pérez Cueva AJ (1991) Analysis of the heat-island effect of the city of Valencia, Spain, through air temperature transects and NOAA satellite data. Theor Appl Climatol 43:195–203. https://doi.org/10.1007/BF00867455
10. Charles N, Reneth M, Shakespear M, Virginia M (2014) Climate change adaptation for rural communities dependent on agriculture and tourism in marginal farming areas of the Hwange District, Zimbabwe. Afr J Agric Res 9:2045–2054. https://doi.org/10.5897/ajar2013.6779
11. Das N, Mondal P, Sutradhar S, Ghosh R (2021) Egypt J Remote Sens Sp Sci 24:131–149. https://doi.org/10.1016/j.ejrs.2020.05.001. Assessment of variation of land use/land cover and its impact on land surface temperature of Asansol subdivision
12. Datta D, Prasad M, Mandla VR (2017) Study of various factors influence on land surface temperature in urban environment. J Urban Environ Eng 11:58–62. https://doi.org/10.4090/juee.2017.v11n1.058062
13. Deilami K, Kamruzzaman M, Liu Y (2018) Urban heat island effect: A systematic review of spatio-temporal factors, data, methods, and mitigation measures. Int J Appl Earth Obs Geoinf 67:30–42. https://doi.org/10.1016/j.jag.2017.12.009
14. Elliott JR, Frickel S (2015) Urbanization as socioenvironmental succession: The case of hazardous industrial site accumulation. Am J Sociol 120:1736–1777. https://doi.org/10.1086/681715
15. Fu P, Weng Q (2016) Remote Sens Environ 175:205–214. https://doi.org/10.1016/j.rse.2015.12.040. A time series analysis of urbanization induced land use and land cover change and its impact on land surface temperature with Landsat imagery
16. Gilani H, Ahmad S, Qazi WA, Abubakar SM, Khalid M (2020) Monitoring of urban landscape ecology dynamics of Islamabad capital territory (ICT), Pakistan, over four decades (1976–2016). Land 9 https://doi.org/10.3390/land9040123
17. Hamza S, Khan I, Lu L, Liu H, Burke F, Nawaz-ul-Huda S, Baqa MF, Tariq A (2021) The Relationship between Neighborhood Characteristics and Homicide in Karachi. Pakistan Sustain 13:5520. https://doi.org/10.3390/su13105520
18. Hasanlou M, Mostofi N (2015) Investigating Urban Heat Island Effects and Relation Between Various Land Cover Indices in Tehran City Using Landsat 8 Imagery. f004. https://doi.org/10.3390/ecrs-1-f004
19. Hashem N, Balakrishnan P (2015) Change analysis of land use/land cover and modelling urban growth in Greater Doha. Qatar Ann GIS 21:233–247. https://doi.org/10.1080/19475683.2014.992369
20. Hoffmann P, Krueger O, Schlünzen KH (2012) A statistical model for the urban heat island and its application to a climate change scenario. Int J Climatol 32:1238–1248. https://doi.org/10.1002/joc.2348
21. Hou H, Wang R, Murayama Y (2019) Scenario-based modelling for urban sustainability focusing on changes in cropland under rapid urbanization: A case study of Hangzhou from 1990 to 2035. Sci Total Environ 661:422–431. https://doi.org/10.1016/j.scitotenv.2019.01.208
22. Huete AR (1988) A soil-adjusted vegetation index (SAVI). Remote Sens Environ 25:295–309. https://doi.org/10.1016/0034-4257(88)90106-X
23. Iram A, Rasool L, Shahzad F, Saeed Y (2012) Impact of urban sprawl on public health: An analysis of Lahore - Pakistan. World Appl Sci J 20:80–86. https://doi.org/10.5829/idosi.wasj.2012.20.01.2806
24. Jensen JR (1983) Urban/ suburban land use analysis. Man. Remote sensing, 2nd Ed. 2, 1571–1666
25. Jimenez-Munoz JC, Sobrino JA, Skokovic D, Mattar C, Cristobal J (2014) Land surface temperature retrieval methods from landsat-8 thermal infrared sensor data. IEEE Geosci Remote Sens Lett 11:1840–1843. https://doi.org/10.1109/LGRS.2014.2312032
26. Kowalski AM (2018) COMPETITIVENESS REPORT 2018 Edited by
27. Li X, Wang Y, Li J, Lei B (2016) Physical and socioeconomic driving forces of land-use and land-cover changes: A Case Study of Wuhan City, China. Discret. Dyn. Nat. Soc. 2016. https://doi.org/10.1155/2016/8061069
28. Lopez TM, Aide TM, Thomlinson JR (2001) Urban expansion and the loss of prime agricultural lands in Puerto Rico. Ambio 30:49–54
29. Ma H, Tong Y (2022) Spatial differentiation of traditional villages using ArcGIS and GeoDa: A case study of Southwest China. Ecol Inf 68:101416. https://doi.org/10.1016/j.ecoinf.2021.101416
30. Mallick J, Kant Y, Bharath BD (2008) Estimation of land surface temperature over Delhi using Landsat-7 ETM+. J Ind Geophys Union 12:131–140
31. Manatsa D, Mushore T, Lenouo A (2017) Improved predictability of droughts over southern Africa using the standardized precipitation evapotranspiration index and ENSO. Theor Appl Climatol 127:259–274. https://doi.org/10.1007/s00704-015-1632-6

32. Mann HB, Whitney DR (1947) On a Test of Whether one of Two Random Variables is Stochastically Larger than the Other. Ann Math Stat 18:50–60. https://doi.org/10.1214/aoms/1177730491
33. Mazvimavi D (2010) Investigating changes over time of annual rainfall in Zimbabwe. Hydrol Earth Syst Sci 14:2671–2679. https://doi.org/10.5194/hess-14-2671-2010
34. McFeeters SK (1996) The use of the Normalized Difference Water Index (NDWI) in the delineation of open water features. Int J Remote Sens 17:1425–1432. https://doi.org/10.1080/01431169608948714
35. Mosammam HM, Nia JT, Khani H, Teymouri A, Kazemi M (2017) Monitoring land use change and measuring urban sprawl based on its spatial forms: The case of Qom city. Egypt J Remote Sens Sp Sci 20:103–116. https://doi.org/10.1016/j.ejrs.2016.08.002
36. Mumtaz F, Tao Y, Leeuw G, De, Zhao L, Fan C, Elnashar A, Bashir B, Wang G, Li LL, Naeem S, Arshad A (2020) Modeling spatio-temporal land transformation and its associated impacts on land surface temperature (LST). Remote Sens. 12. https://doi.org/10.3390/RS12182987
37. Mushore TD, Mutanga O, Odindi J, Dube T (2018) Determining extreme heat vulnerability of Harare Metropolitan City using multispectral remote sensing and socio-economic data. J Spat Sci. https://doi.org/10.1080/14498596.2017.1290558
38. Mushore TD, Odindi J, Dube T, Mutanga O (2017) Prediction of future urban surface temperatures using medium resolution satellite data in Harare metropolitan city. Zimbabwe Build Environ 122:397–410. https://doi.org/10.1016/j.buildenv.2017.06.033
39. Nowak DJ, Walton JT (2005) Projected urban growth (2000–2050) and its estimated impact on the US forest resource. J For 103:383–389. https://doi.org/10.1093/jof/103.8.383
40. Pal S, Ziaul S (2017) Detection of land use and land cover change and land surface temperature in English Bazar urban centre. Egypt J Remote Sens Sp Sci 20:125–145. https://doi.org/10.1016/j.ejrs.2016.11.003
41. Peña MA (2008) Relationships between remotely sensed surface parameters associated with the urban heat sink formation in Santiago. Chile Int J Remote Sens 29:4385–4404. https://doi.org/10.1080/01431160801908137
42. Prasad P, Joseph V, Chandra P, Kotha M (2022) Ecological Informatics Evaluation and comparison of the earth observing sensors in land cover / land use studies using machine learning algorithms. Ecol Inf 68:101522. https://doi.org/10.1016/j.ecoinf.2021.101522
43. Reddy CV, Kumara MP, Mandlaa VR (2014) Influence of land surface temperature and CO2 on urban environment by using landsat-8, in: ISPRS TC VIII International Symposium on "Operational Remote Sensing Applications: Opportunities, Progress and Challenges, Paraíba, Brazill
44. Saitoh TS, Shimada T, Hoshi H (1996) Modeling and simulation of the Tokyo urban heat island. Atmos Environ 30:3431–3442. https://doi.org/10.1016/1352-2310(95)00489-0
45. Sayemuzzaman M, Jha MK (2014) Modeling of Future Land Cover Land Use Change in North Carolina Using Markov Chain and Cellular Automata Model. Am J Eng Appl Sci 7:295–306. https://doi.org/10.3844/ajeassp.2014.295.306
46. SHAPIRO SS, WILK MB (1965) An analysis of variance test for normality (complete samples)†. Biometrika 52:591–611. https://doi.org/10.1093/biomet/52.3-4.591
47. Shi L, Taubenböck H, Zhang Z, Liu F, Wurm M (2019) Urbanization in China from the end of 1980s until 2010 – spatial dynamics and patterns of growth using EO-data. Int J Digit Earth 12:78–94. https://doi.org/10.1080/17538947.2017.1400599
48. Smakhtin VU, Hughes DA (2007) Automated estimation and analyses of meteorological drought characteristics from monthly rainfall data. Environ Model Softw 22:880–890. https://doi.org/10.1016/j.envsoft.2006.05.013
49. Sobrino JA, Jiménez-Muñoz JC, Paolini L (2004) Land surface temperature retrieval from LANDSAT TM 5. Remote Sens Environ 90:434–440. https://doi.org/10.1016/j.rse.2004.02.003
50. Sobrino JA, Oltra-Carrió R, Sòria G, Jiménez-Muñoz JC, Franch B, Hidalgo V, Mattar C, Julien Y, Cuenca J, Romaguera M, Gómez JA, de Miguel E, Bianchi R, Paganini M (2013) Evaluation of the surface urban heat island effect in the city of Madrid by thermal remote sensing. Int J Remote Sens 34:3177–3192. https://doi.org/10.1080/01431161.2012.716548
51. Stathopoulou M, Cartalis C, Chrysoulakis N (2006) Using midday surface temperature to estimate cooling degree-days from NOAA-AVHRR thermal infrared data: An application for Athens. Greece Sol Energy 80:414–422. https://doi.org/10.1016/j.solener.2005.02.004
52. Sultana SR, Ali A, Ahmad A, Mubeen M, Zia-Ul-Haq M, Ahmad S, Ercisli S, Jaafar HZE (2014) Normalized difference vegetation index as a tool for wheat yield estimation: A case study from Faisalabad, Pakistan. Sci. World J. 2014. https://doi.org/10.1155/2014/725326
53. Tariq A, Riaz I, Ahmad Z, Amin M, Kausar R, Andleeb S, Farooqi MA, Rafiq M (2020) Land surface temperature relation with normalized satellite indices for the estimation of spatio-temporal trends in temperature among various land use land cover classes of an arid Potohar region using Landsat data. Environ Earth Sci 79:1–15. https://doi.org/10.1007/s12665-019-8766-2
54. Tariq A, Shu H (2020) Pakistan Remote Sens 12:1–23. https://doi.org/10.3390/rs12203402. CA-Markov chain analysis of seasonal land surface temperature and land use landcover change using optical multi-temporal satellite data of Faisalabad

55. Tariq A, Shu H, Siddiqui S, Imran M, Farhan M (2021) Geogr Environ Sustain 14:41–52. https://doi.org/10.24057/2071-9388-2020-117. Monitoring Land Use And Land Cover Changes Using Geospatial Techniques, A Case Study Of Fateh Jang, Attock, Pakistan
56. Triantakonstantis D, Mountrakis G (2012) Urban Growth Prediction: A Review of Computational Models and Human Perceptions. J Geogr Inf Syst 04:555–587. https://doi.org/10.4236/jgis.2012.46060
57. Tucker CJ (1979) Red and photographic infrared linear combinations for monitoring vegetation. Remote Sens Environ 8:127–150. https://doi.org/https://doi.org/10.1016/0034-4257(79)90013-0
58. Walter V (2004) Object-based classification of remote sensing data for change detection. ISPRS J Photogramm Remote Sens 58:225–238. https://doi.org/10.1016/j.isprsjprs.2003.09.007
59. Wang X, Chen D, Ren Z (2010) Assessment of climate change impact on residential building heating and cooling energy requirement in Australia. Build Environ 45:1663–1682. https://doi.org/10.1016/j.buildenv.2010.01.022
60. Weng Q, Liu H, Lu D (2007) Assessing the effects of land use and land cover patterns on thermal conditions using landscape metrics in city of Indianapolis, United States. Urban Ecosyst 10:203–219. https://doi.org/10.1007/s11252-007-0020-0
61. Weng Q, Lu D, Schubring J (2004) Estimation of land surface temperature-vegetation abundance relationship for urban heat island studies. Remote Sens Environ 89:467–483. https://doi.org/10.1016/j.rse.2003.11.005
62. Wilson M (2020) Climate Change. Can Vet J = La Rev Vet Can 61:225
63. Xu LY, Xie XD, Li S (2013) Correlation analysis of the urban heat island effect and the spatial and temporal distribution of atmospheric particulates using TM images in Beijing. Environ Pollut 178:102–114. https://doi.org/10.1016/j.envpol.2013.03.006
64. Xue J, Su B (2017) Significant remote sensing vegetation indices: A review of developments and applications. J. Sensors 2017. https://doi.org/10.1155/2017/1353691
65. Yang F (2004) Turbo decoder using local subsidiary maximum likelihood decoding in prior estimation of the extrinsic information. J Electron 21:89–96. https://doi.org/10.1007/BF02687822
66. Yuan F, Bauer ME (2007) Comparison of impervious surface area and normalized difference vegetation index as indicators of surface urban heat island effects in Landsat imagery. Remote Sens Environ 106:375–386. https://doi.org/10.1016/j.rse.2006.09.003
67. Zahoor B, Liu X, Dai Y, Kumar L, Songer M (2022) Ecological Informatics Identifying the habitat suitability and built-in corridors for Asiatic black bear (Ursus thibetanus) movement in the northern highlands of Pakistan. Ecol Inf 68:101532. https://doi.org/10.1016/j.ecoinf.2021.101532
68. Zha Y, Gao J, Ni S (2003) Use of normalized difference built-up index in automatically mapping urban areas from TM imagery. Int J Remote Sens 24:583–594. https://doi.org/10.1080/01431160304987

Figures

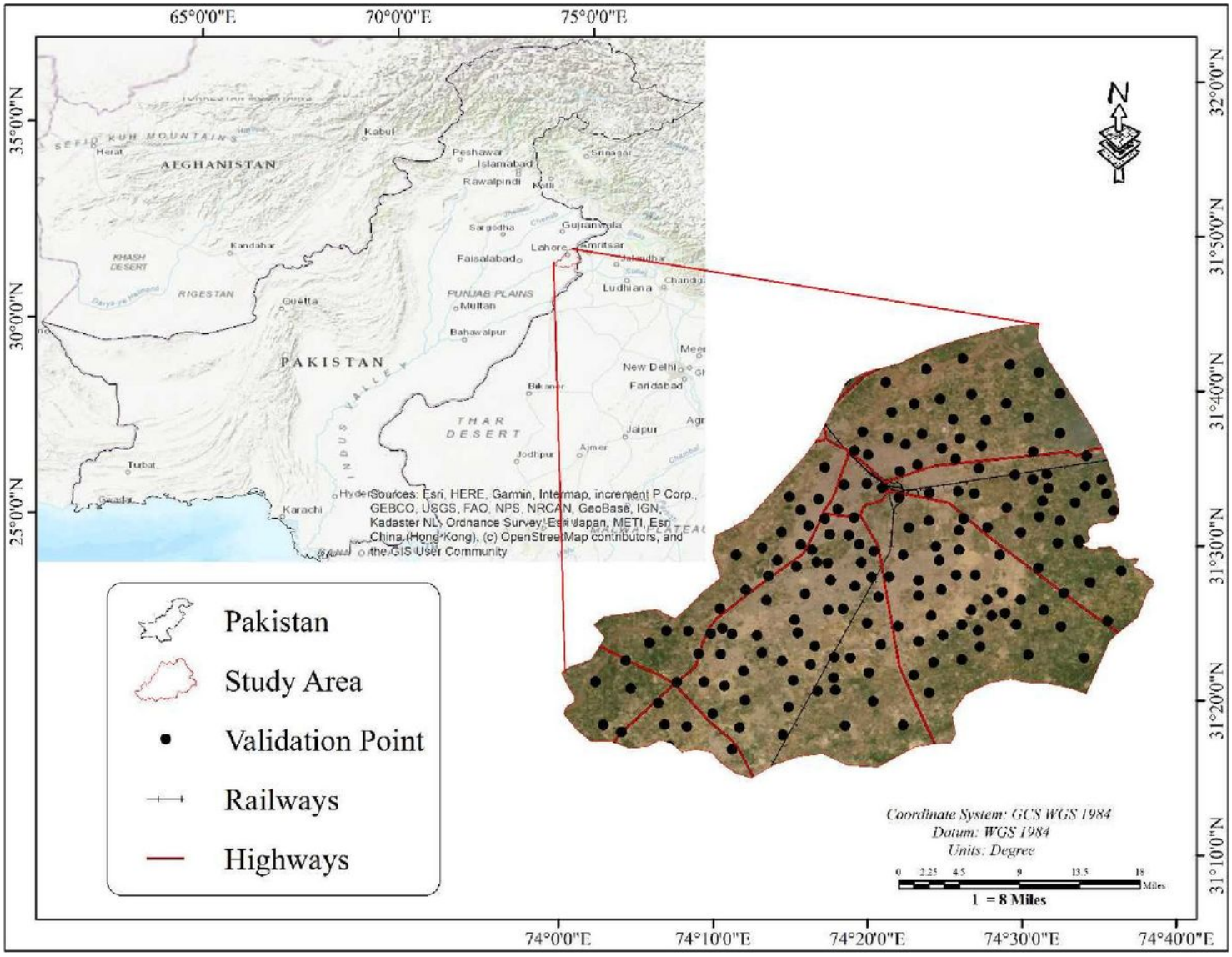

Figure 1

Geographical Location of Lahore City with validation points.

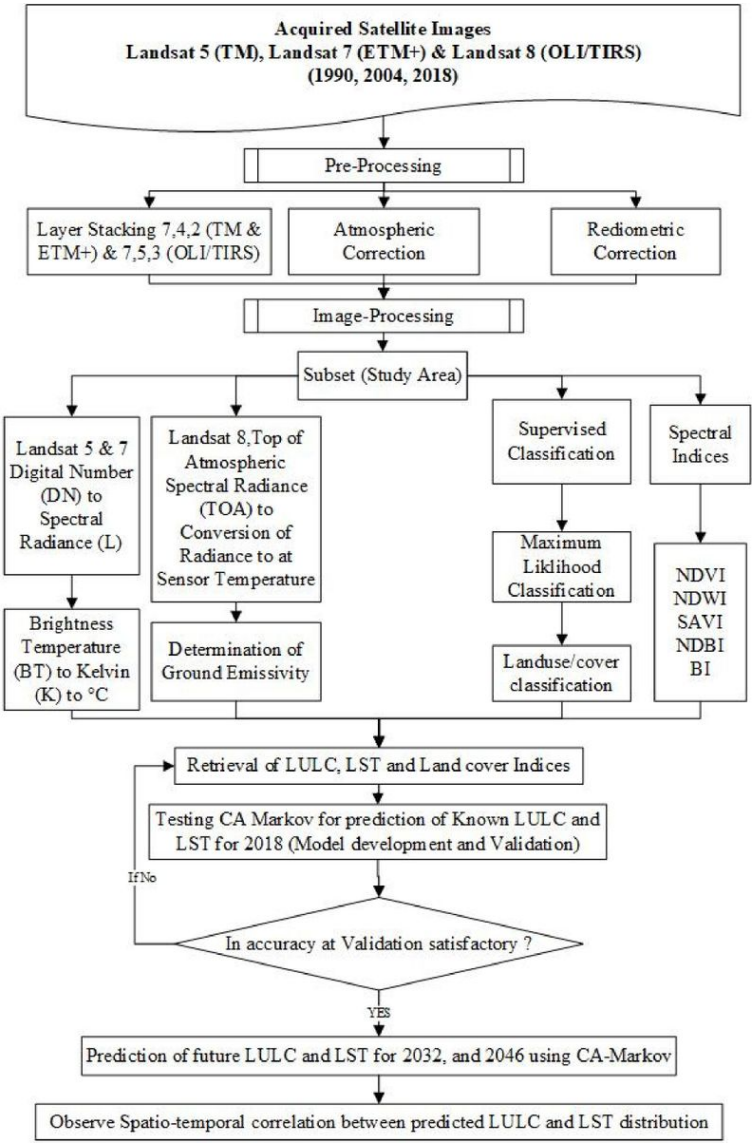

Figure 2

Flowchart explains the methodology in this study.

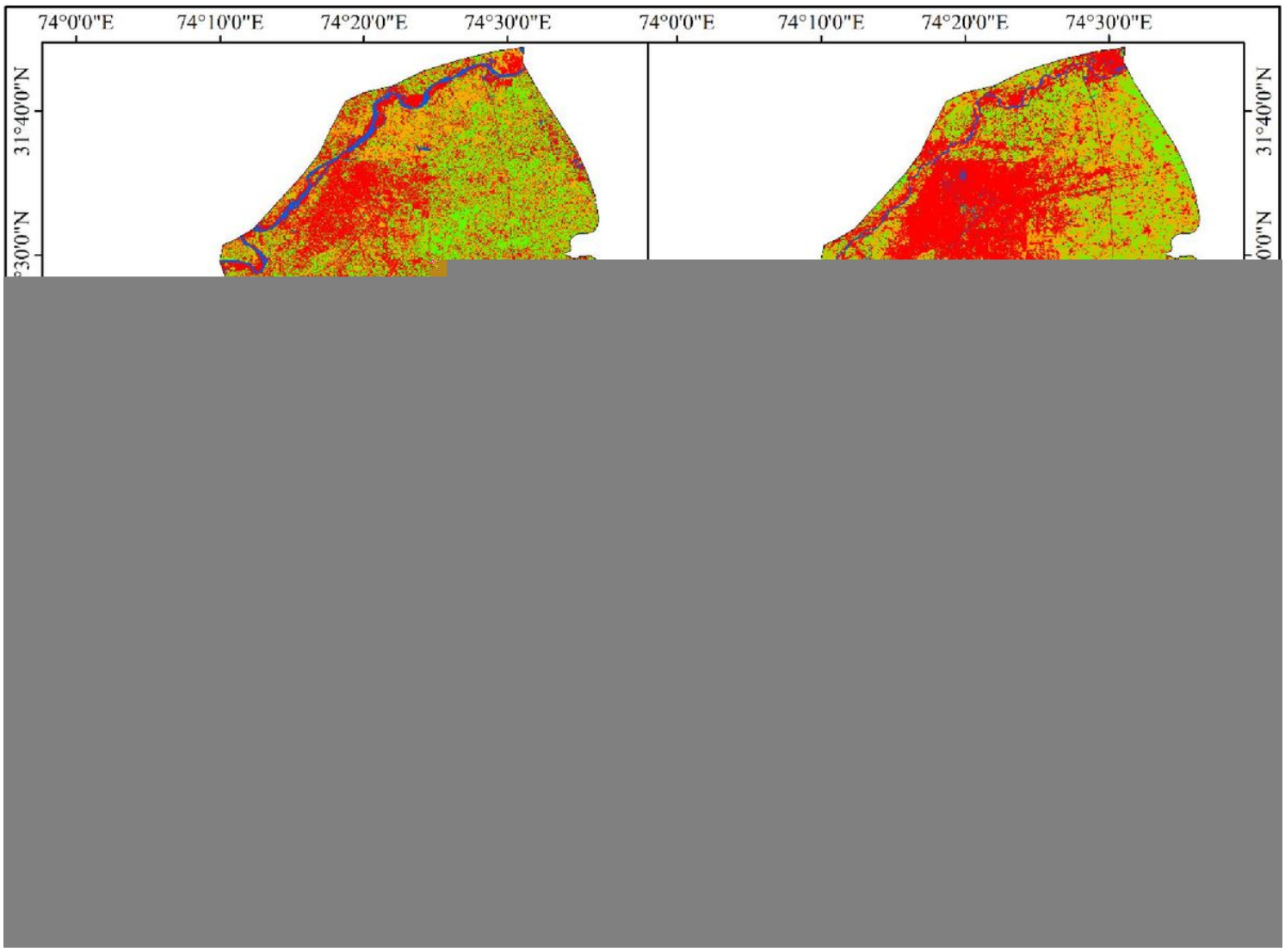

Figure 3

Land use map of Lahore from 1990-2018 and area in km^2 (a) 1990 (b) 2004 (c) 2018.

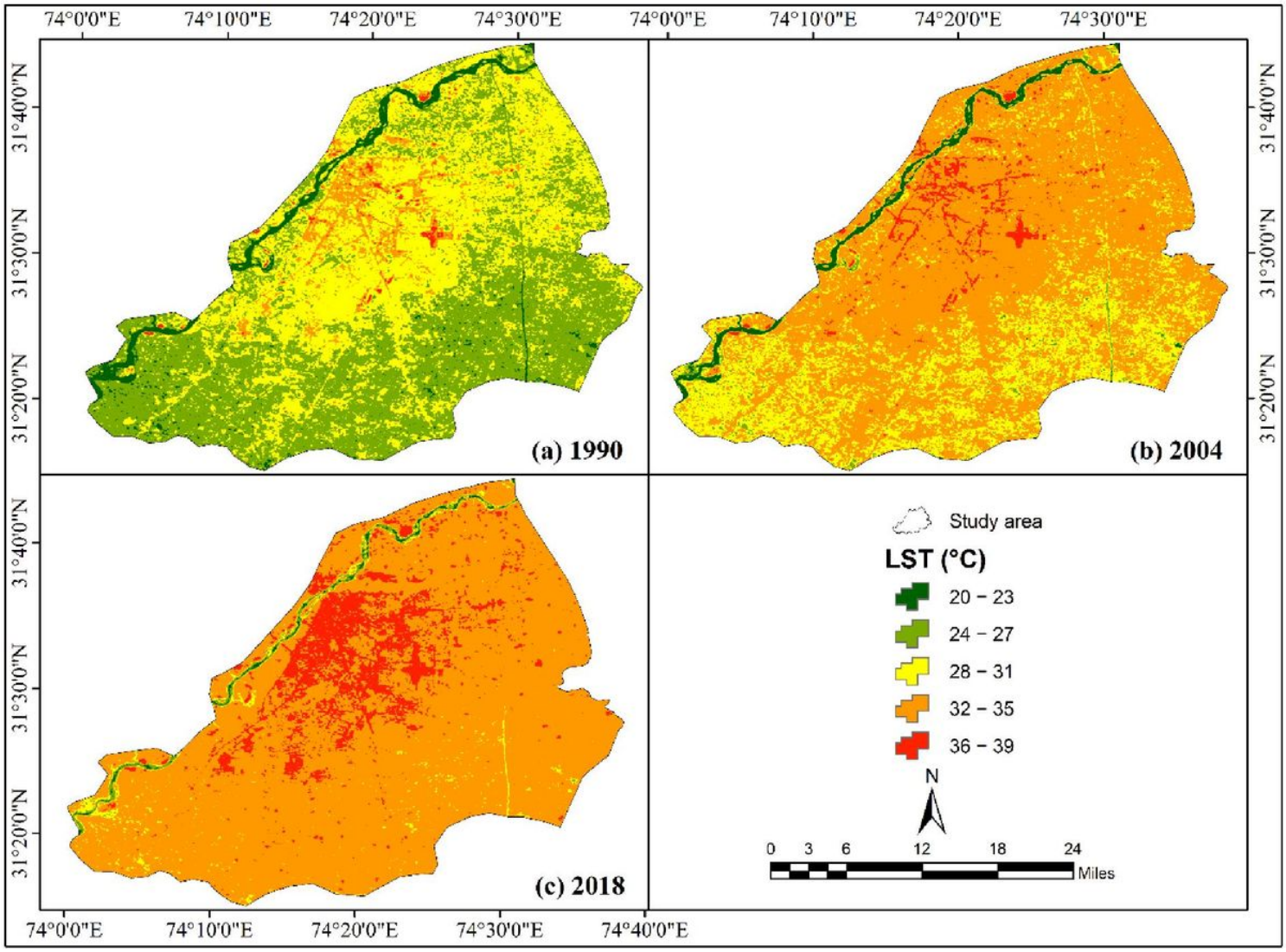

Figure 4

Spatio-temporal changes and mapping of LST were observed in (a) 1990, (b) 2004, (c) 2018.

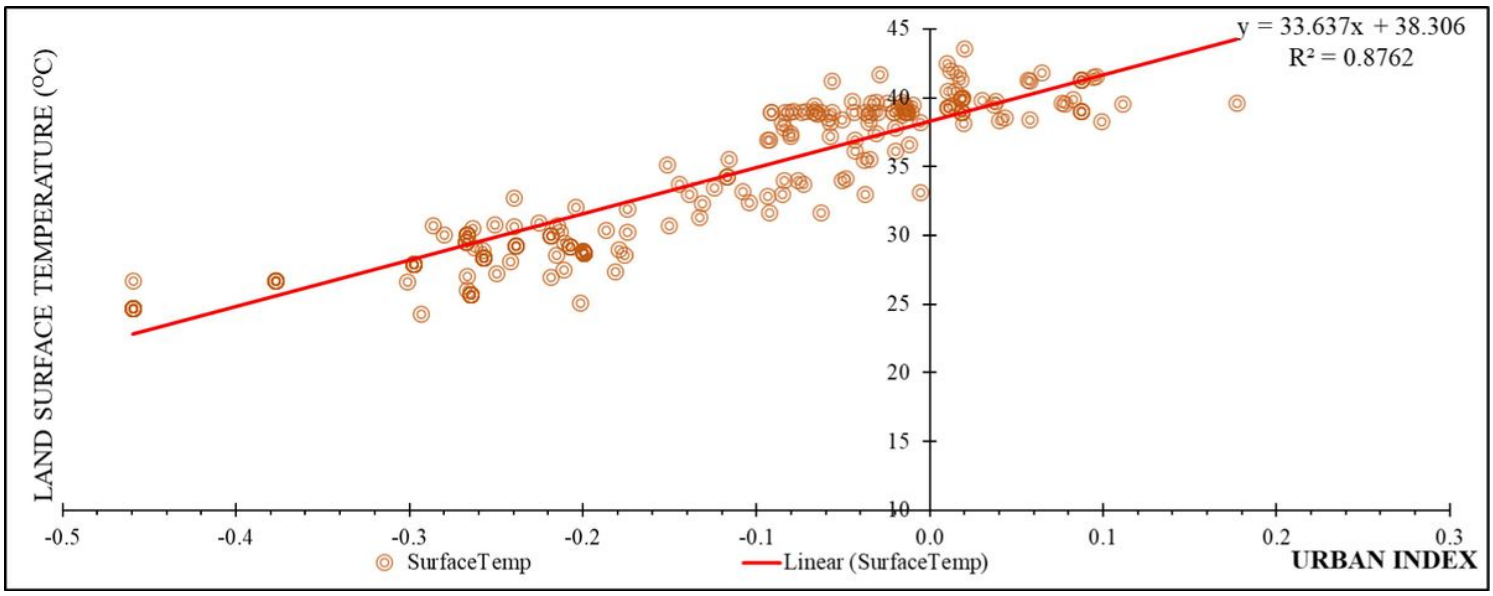

Figure 5

Using a linear model to predict LST from the UI.

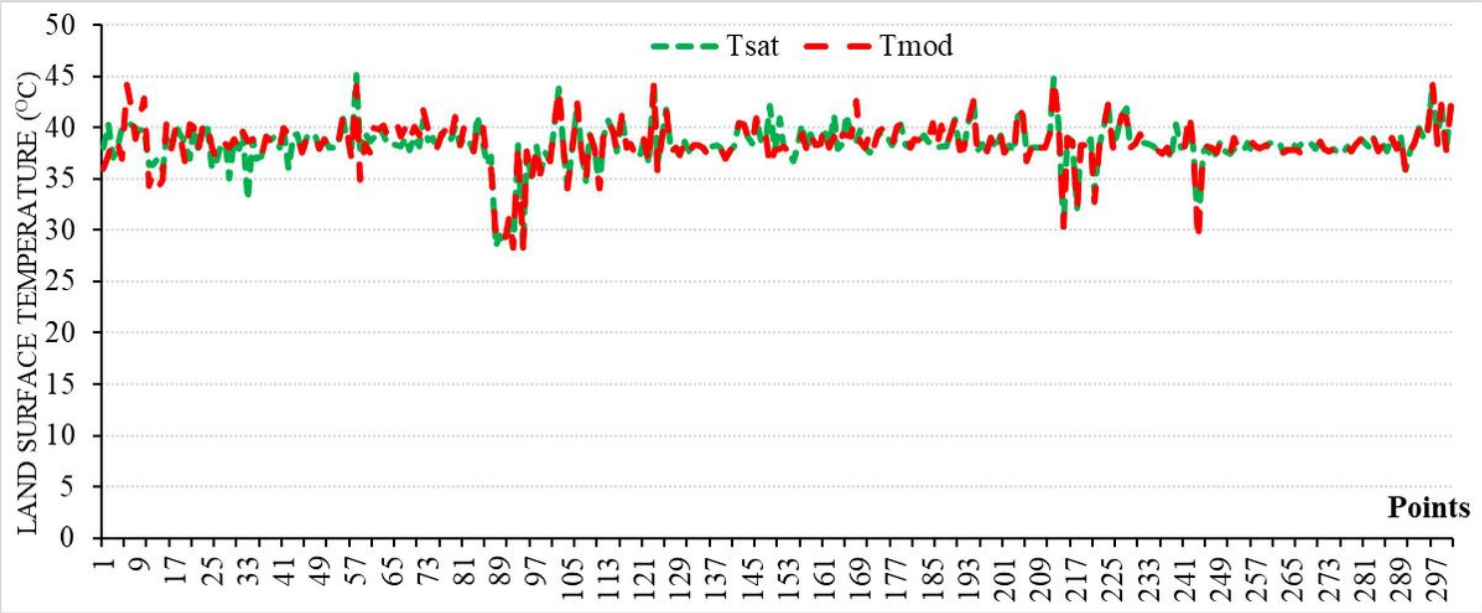

Figure 6

Comparison of surface temperature derived from thermal band with UI.

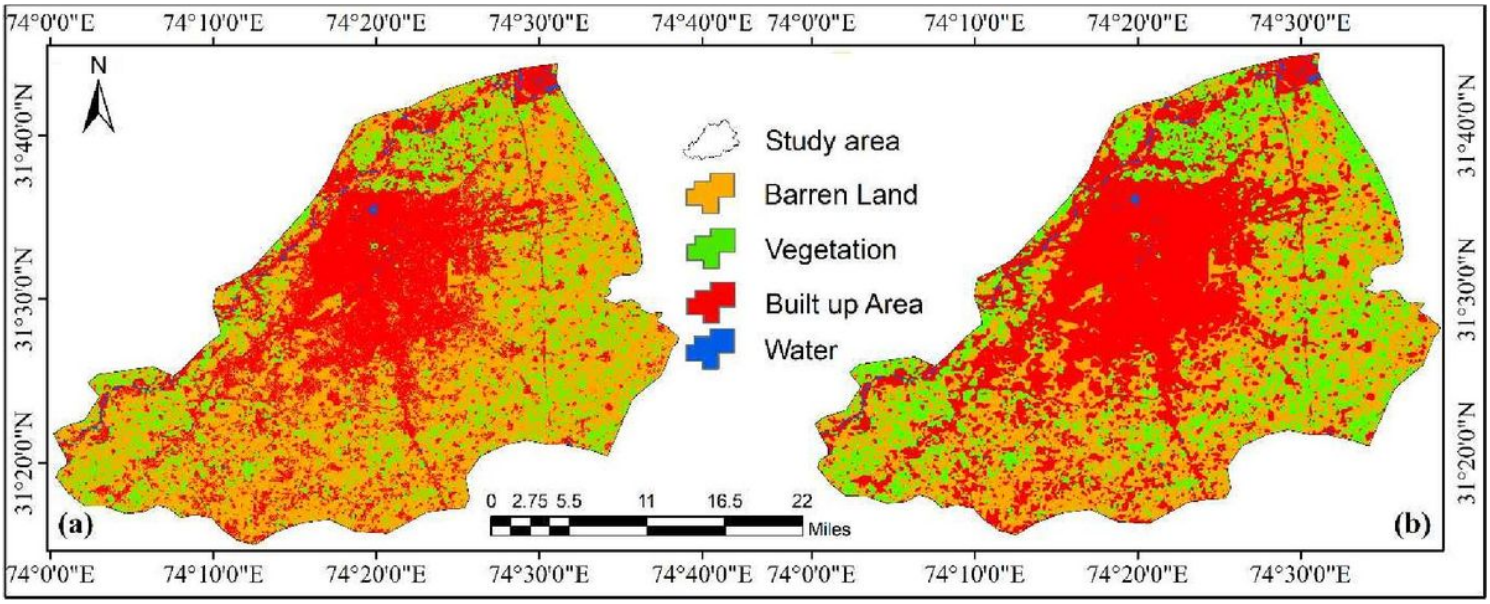

Figure 7

2018 LULC mapping with (**a**) MLC and (**b**) CA-Markov-Chain prediction.

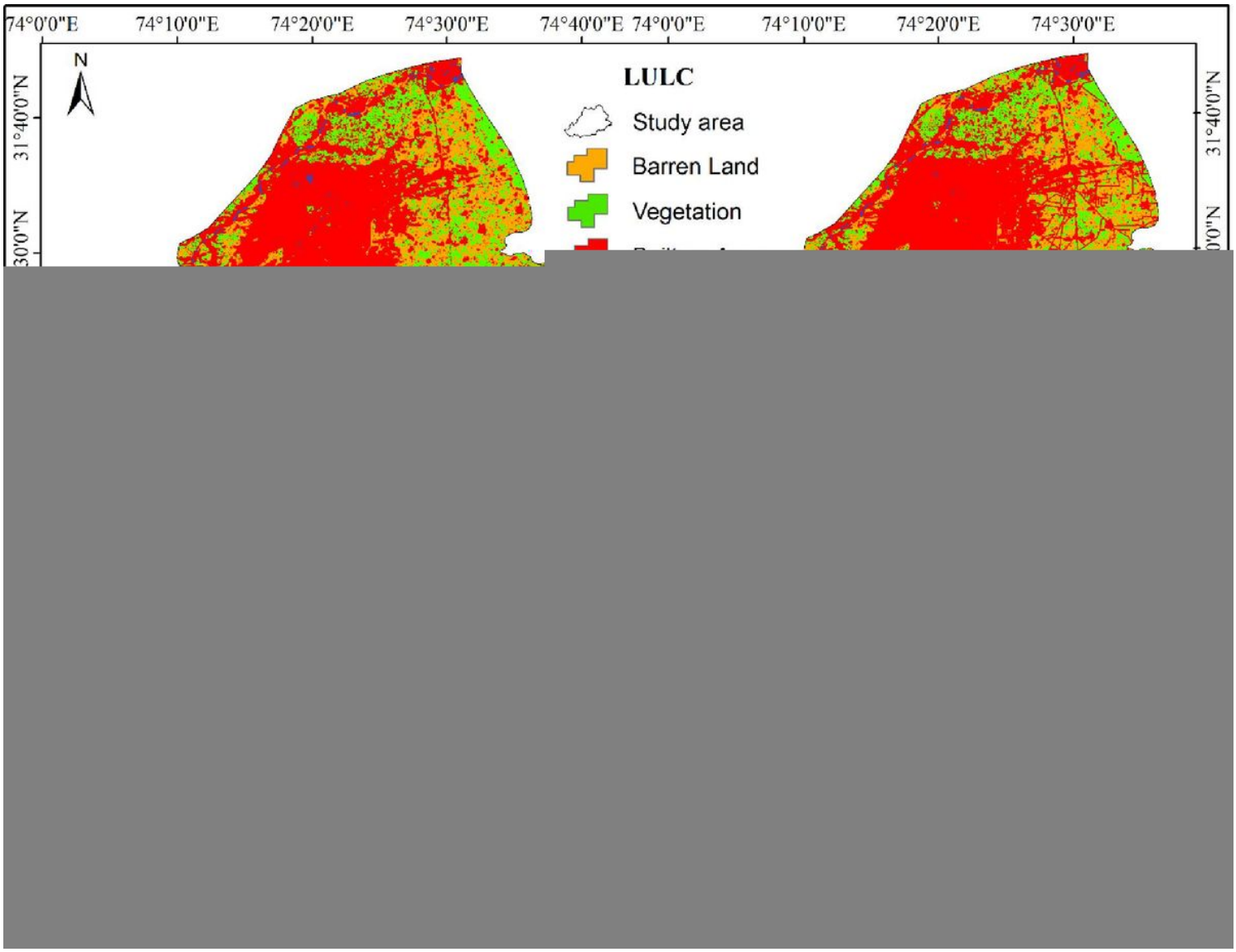

Figure 8

Predicted LULC types and LST distribution in 2032 and 2046.